

A simple and objective method to partition evapotranspiration into transpiration and evaporation at eddy-covariance sites



Xi Li^{a,b,*}, Pierre Gentine^{b,*}, Changjie Lin^c, Sha Zhou^b, Zan Sun^a, Yi Zheng^d, Jie Liu^a, Chunmiao Zheng^{a,d}

^a Institute of Water Sciences, College of Engineering, Peking University, Beijing, 100871, China

^b Department of Earth and Environmental Engineering, Columbia University, New York, New York, 10027, USA

^c State Key Laboratory of Hydroscience and Engineering, Department of Hydraulic Engineering, Tsinghua University, Beijing, 100084, China

^d Guangdong Provincial Key Laboratory of Soil and Groundwater Pollution Control, School of Environmental Science and Engineering, Southern University of Science and Technology, Shenzhen, 518055, China

ARTICLE INFO

Keywords:

Evapotranspiration partitioning
Ecosystem conductance
Soil moisture
VPD

ABSTRACT

Separating evapotranspiration (ET) into evaporation (E) and transpiration (T) is challenging but key for a better understanding and prediction of the hydrological cycle and plant water use. In this study, flux data at 30 routine eddy-covariance sites were used to develop a new and simple method for ET partitioning based on the separation of soil and canopy conductances, with the main assumption that the latter is proportional to gross primary productivity (GPP). The result of $T:ET$ across different plant functional types (PFTs) was consistent with recent modeling or empirical results. The mean annual $T:ET$ was highest for evergreen needleleaf forests (0.75 ± 0.17), followed by croplands (0.62 ± 0.16) and grasslands (0.56 ± 0.15). The leaf area index (LAI) was shown to explain only small (20%) variations of mean annual $T:ET$ across sites. However, at each site, the correlation of $T:ET$ with LAI was strong at the seasonal scale, where $T:ET$ increased nonlinearly with LAI. The results did not show significant relationship of $T:ET$ with long-term mean precipitation across sites at multiyear timescales. However, the partitioned soil evaporation after each precipitation pulse is consistent with three-stage soil evaporation theory. This ET partitioning method is an objective assessment as it is mainly data-driven. The procedure to apply this method is also simple so it can be readily applied to global flux tower networks at different temporal and spatial scales, enabling continuous estimation of $T:ET$ to monitor ecosystem dynamics and hydrological responses to environmental change.

1. Introduction

Evapotranspiration (ET), consisting of canopy interception evaporation, evaporation from soil and wet surfaces, and transpiration by plants, is a key component of the global hydrological cycle (Lemordant et al., 2018). As the largest component of ET , transpiration serves as a central linkage between carbon, water, and energy fluxes (Katul et al., 2012) and accounts for a large fraction (40–90%) of the annual land surface water fluxes (Jasechko et al., 2013; Schlesinger and Jasechko, 2014; Wang et al., 2014; Good et al., 2015; Zhou et al., 2016). Numerous components of the global hydrological cycle, such as atmospheric humidity, precipitation, streamflow, soil moisture and groundwater dynamics, are strongly affected by transpiration (Farley et al., 2005; Weng and Luo, 2008; Maxwell and Condon, 2016; Green et al., 2017; Li et al., 2017). In addition, transpiration is also required to

understand plant water use efficiency (Mastrotheodoros et al., 2017) as well as stomatal responses to environmental stresses (Lee et al., 2010). Separating evaporation and transpiration is also essential to improve the modeling of land-atmosphere interactions (Kool et al., 2014), and in particular to predict the temporal response to droughts across biomes (Williams et al., 2016; Konings et al., 2017).

The ratio between transpiration and evapotranspiration, denoted $T:ET$, has been investigated using several direct and indirect methods from plot to ecosystem scale, including stable isotope techniques (Zhang et al., 2011; Good et al., 2014; Wen et al., 2016; Lu et al., 2017), sap flux or eddy-covariance techniques (Baldocchi and Ryu, 2011; Cammalleri et al., 2013), modeling (Tian et al., 2013; Maxwell and Condon, 2016; Diarra et al., 2017; Fatichi and Pappas, 2017; Sun et al., 2018), and eddy-covariance high-frequency correlation approach (Scanlon and Sahu, 2008; Scanlon and Kustas, 2010; Zhou et al., 2016).

* Corresponding authors at: Department of Earth and Environmental Engineering, Columbia University, New York, NY, 10027, USA.

E-mail addresses: lixi09@pku.edu.cn (X. Li), pg2328@columbia.edu (P. Gentine).

The isotopic technique is considered a relatively direct measurement of evaporation and transpiration ratio and is based on the differences in the isotopic signature of water vapor as a result of E or T (Risi et al., 2013; Kool et al., 2014). This method is costly and labor-intensive, making continuous measurements extremely complicated (Wang et al., 2012; Griffis, 2013). In addition, it requires assumptions about the isotope compositions of the leaves, which are hard to measure at the ecosystem scale, especially continuously in time. Sap flow measurement is another method to directly measure transpiration rate (Cammalleri et al., 2013). However, the sap flow velocity measured in individual plants is not typically representative of the whole ecosystem due to the species heterogeneity. Eddy-covariance techniques can also be used by assuming that the water fluxes measured both above the canopy and understory represent ET and E , respectively (Balocchi and Ryu, 2011). However, this method ignores the transpiration of understory plants, and may underestimate $T:ET$. Numerous models have also been used to estimate ET partitioning including mechanistic and empirical models that employ either numerical or analytical solutions. Yet, these models require complex parameterizations and still require validation (Kool et al., 2014). To overcome some of the aforementioned limitations, correlation-based ET partitioning approaches have been proposed, using high-frequency eddy-covariance data. They assume that the relation between ET and CO_2 is due to a mixture of stomatal fluxes (T and photosynthesis) and non-stomatal fluxes (E and respiration) (Scanlon and Sahu, 2008). The value of this method is that it can be used with regular eddy-covariance measurements (at high frequency e.g. 10–20 Hz), but it relies on the prescription of the leaf-level water use efficiency (WUE), which is unknown a priori, and which varies across species within the flux footprint and with environmental conditions, even during a single day. Zhou et al. (2016) also proposed a new method for ET partitioning based on the concept of underlying water use efficiency (uWUE) by assuming that the maximum uWUE is related to T only, as E can be neglected during peak growing seasons, while more typical uWUE reflects total ET . While this method uses half-hourly eddy-covariance data and is simple to apply in practice, it assumes a specific dependence on VPD (square root of VPD) and ignores entirely soil evaporation during the peak growing season. The latter assumption may be invalid and would overestimate $T:ET$ in water-limited cases. Therefore, simple and objective methods to estimate ET partitioning at routine eddy-covariance are still lacking.

Evaporation and transpiration have different responses to environmental drivers as transpiration is only associated with vegetation and mostly controlled by stomata regulation, while soil evaporation only relies on the soil and environmental conditions, reflected by soil conductance. Following this idea, dual-source evapotranspiration models (Shuttleworth and Wallace, 1985; Lhomme and Chehbouni, 1999) separate ecosystem surface conductance into canopy conductance and soil conductance to separate T and E . Based on generalizations of empirical stomatal conductance models (Ball et al., 1987; Leuning, 1995) and the optimal stomatal model (Medlyn et al., 2011), Lin et al. (2018) proposed a best-fit ecosystem-level conductance model using hourly flux data, which described the behavior of ecosystem-level conductance and its response to VPD and soil moisture. In this best-fit model, the retrieved ecosystem-level conductance includes both soil and canopy contributions corresponding to ET partitioning. Here, we use this best-fit model, separating the total surface conductance into soil and canopy portions, in order to estimate $T:ET$. Compared to regular dual-source models with many atmospheric and vegetation dependent parameters, the soil and canopy conductances presented here are directly fitted to the data so that they are data constrained rather than parameterization driven.

Beyond identifying E and T separately, it is also critical to find the factors controlling the variability of $T:ET$ across biomes. Recently, transpiration ratio has been directly linked to phenology at the seasonal timescale via factors like leaf area index (LAI) and enhanced vegetation index (EVI) (Wang et al., 2014; Zhou et al., 2016; Wei et al., 2017).

Zhou et al. (2016) found that EVI could explain about 75% of the variation in $T:ET$ and the coefficient of determination between EVI and $T:ET$ could be even higher over croplands. However, the previous work on the link of transpiration ratio and LAI at spatial scale is inconsistent. Wang et al. (2014) estimated that LAI could explain 43% of the global $T:ET$ spatial variability, much lower than the estimates of seasonal LAI impact mentioned above. Fatichi and Pappas (2017) also found a lack of sensitivity of $T:ET$ to growing season LAI across sites using a mechanistic ecohydrological model. These inconsistent results motivate more direct assessments of the LAI control on $T:ET$. Besides vegetation, climatic factors such as precipitation could also affect the dynamics of $T:ET$. Although Fatichi and Pappas (2017) and Schlesinger and Jasechko (2014) have both showed that $T:ET$ appears to be independent of mean annual precipitation across sites, the frequency of precipitation could also affect the ET partitioning. The time after precipitation can also be considered a proxy for the contribution of evaporation to ET (Knauer et al., 2017), and analyzing the variation of evaporation with precipitation pulses could be helpful to further validate ET partitioning methods.

The main objective of this study is therefore to develop a new simple and objective method to partition ET by separating the canopy and soil conductances using widely accessible half-hourly eddy-covariance flux data. Our objectives are threefold: (1) to separate ET using the separation of canopy and soil conductances via two different types of ecosystem conductance models; (2) to evaluate whether the separated canopy and soil conductances are broadly consistent with physical understanding; and (3) to evaluate the dependence of ET partitioning on LAI and environmental drivers. The proposed method for ET partitioning can be applied to global flux tower networks and enables characterization of $T:ET$ and its temporal variations.

2. Materials & methods

2.1. FLUXNET dataset

Half-hourly or hourly eddy-covariance data were taken from the FLUXNET2015 Tier 1 dataset (<http://fluxnet.fluxdata.org>). We selected sites with a data record covering at least 4 years, and with meteorological data, including radiation, precipitation, air humidity, and measurement height. Available soil moisture and photosynthetically active radiation (PAR) data were also needed, and 30 sites were therefore selected (Table S1), comprising seven croplands (CRO) sites, three deciduous broadleaf forests (DBF) sites, one evergreen broadleaf forests (EBF) sites, ten evergreen needleleaf forests (ENF) sites, seven grasslands (GRA) sites, and two woody savannas (WSA) sites. Flux data underwent standard processing, including friction velocity filtering, gap filling, and flux partitioning (Pastorello et al., 2014). Specifically, in terms of gross primary production (GPP), we used the variable “GPP_NT_VUT_REF” in the dataset, which is based on the nighttime respiration partitioning method. Only measured data without gap-filled were used in this study.

Data screening and quality control were performed to select hourly observations following processes similar to previous studies (Zhou et al., 2016; Knauer et al., 2017; Medlyn et al., 2017). First, we excluded data with relative humidity exceeding 95% to avoid the high likelihood of dew evaporation (Knauer et al., 2017), as it can strongly impact ET measurements. Second, data during rainy hours and within 6 h after rainfall were also removed to avoid interception evaporation and sensor saturation at high relative humidity. Third, only daytime data with sensible heat flux larger than 5 W m^{-2} and incoming short-wave radiation larger than 50 W m^{-2} were used to avoid stable boundary layer conditions. Finally, times with negative GPP, ET , and VPD were excluded. Half-hourly data were aggregated into hourly data in order to reduce noise. Data availability after filtering is given in Table S2 at each site. In this study, daily values were estimated only for days when there were at least 8 measured daylight points.

2.2. Ecosystem conductance G_s calculation

The ecosystem conductance (G_s) was calculated by inverting the Penman-Monteith equation (Penman, 1948; Monteith, 1965) using eddy-covariance data:

$$G_s = \frac{\gamma G_a LE}{\Delta(R_n - G) + \rho c_p G_a VPD_a - (\Delta + \gamma)LE} \quad (1)$$

Where γ is the psychrometric constant (kPa K^{-1}), G_a is the aerodynamic conductance (m s^{-1}), Δ is the slope of the saturation vapor pressure curve (kPa K^{-1}), LE is the latent heat flux (W m^{-2}), R_n is the net radiation (W m^{-2}), G is the ground heat flux (W m^{-2}), ρ is the air density (kg m^{-3}), c_p is the specific heat of air ($\text{J kg}^{-1} \text{K}^{-1}$), VPD_a (kPa) is the atmospheric vapor pressure deficit defined as the difference between saturated vapor pressure at ambient temperature and actual vapor pressure. The calculation of G_a followed the procedures described in Lin et al. (2018) including the corrections for stability. The impact of errors in G_a has been tested and found small compared to other factors (Novick et al., 2016). The unit for G_s in this equation is m s^{-1} but this was then transformed to $\text{mol m}^{-2} \text{s}^{-1}$ using the ideal gas law (Lin et al., 2018).

The PM equation assumes that the energy balance at the land surface is closed, which is typically violated for the observed flux data (Foken, 2008). Therefore, we evaluated the impact of energy balance closure for each site using the regression coefficients (slope and intercept) from the ordinary least squares relationship between the hourly flux variables of ($LE + H$) against the available energy ($R_n - G$). We also tested the uncertainty of the unclosed energy balance on the G_s estimates derived from the PM equation and the corresponding $T:ET$ results based on three hypothetical cases to attribute the residual of the energy balance closure. In the first case, all errors come from H by assuming that both ($R_n - G$) and LE are correct. This case is implied by Eq. (1). In the second case, all errors come from LE by assuming that both ($R_n - G$) and H are correct. In this case, we recalculate LE as $LE = (R_n - G - H)$. In the third case, all errors come from ($R_n - G$) by assuming that both LE and H are correct. In this case, we recalculate ($R_n - G$) as $R_n - G = LE + H$. The entire algorithm has been rerun to calculate G_s and corresponding $T:ET$ in each case.

Hourly G_s can include outliers even after data screening. To exclude the outliers, we calculated the median absolute deviation (MAD) using a 10-hour moving window to determine the outliers. G_s is defined as an outlier when it falls outside the local median $\pm 3\text{MAD}$ range over a window length (Papale et al., 2006; Leys et al., 2013).

Considering the fact that the meteorological conditions at the canopy surface are physiologically more relevant than those in the air above the canopy (Knauer et al., 2017), we calculated the inferred leaf-level VPD at the ecosystem scale (VPD_l) using the definition of latent heat flux across the big-leaf interface instead of the meteorological atmospheric VPD (VPD_a).

$$VPD_l = \frac{\gamma LE}{\rho c_p G_s} \quad (2)$$

VPD_l corresponds to the VPD gradient from the big leaf to the weather station measurement. This method is adapted from Lin et al. (2018), where they discuss why VPD_l performs better when depicting behaviors of ecosystem conductance.

2.3. Separating soil and canopy conductances

The ecosystem conductance G_s inverted from the PM equation is the sum of canopy conductance (G_{veg}), soil conductance (G_{soil}), and conductance from water intercepted by the canopy. In this study, we excluded data during rainy hours and within 6 h after rainfall to avoid the influence of interception. As such, G_s only reflects contributions from soil evaporation and canopy transpiration.

$$G_s = G_{soil} + G_{veg} \quad (3)$$

To separate G_{soil} and G_{veg} , we here introduce a recent ecosystem conductance model described in Lin et al. (2018), which generalized Leuning's model (Leuning, 1995) and Medlyn's model (Medlyn et al., 2011):

$$G_s = G_0 + G_1 \frac{GPP}{VPD_l^m} \quad (4)$$

where G_0 ($\text{mol m}^{-2} \text{s}^{-1}$), G_1 ($\text{kPa}^m \text{ mol } \mu\text{mol}^{-1}$) and m are fitted parameters at the ecosystem level, and GPP is gross primary production ($\mu\text{mol m}^{-2} \text{s}^{-1}$). In contrast to Leuning's model and Medlyn's model, the exponent of VPD_l in Eq. (4), m , is allowed to vary across ecosystems to a best-fitted value, rather than a fixed one of 0.5. The model in Eq. (4) is denoted as the m -order VPD model.

We here assume that only canopy conductance is related to photosynthesis (e.g. GPP). Therefore, the term $G_1 \frac{GPP}{VPD_l^m}$ in Eq. (4), which is proportional to GPP, only reflects canopy conductance. Moreover, as stated in Lin et al. (2018), G_0 reflects both soil conductance and minimum canopy conductance ($G_{veg, min}$). However, $G_{veg, min}$, which reflects cuticular and epidermal losses, is negligible compared to soil evaporation, even in very dry conditions (Lin et al., 2015; Knauer et al., 2017; Medlyn et al., 2017). Therefore, we finally decompose G_s into G_{soil} and G_{veg} :

$$G_{soil} = G_0 \quad (5)$$

$$G_{veg} = G_1 \frac{GPP}{VPD_l^m} \quad (6)$$

Both soil moisture supply and atmospheric water demand (directly related to VPD) independently limit canopy conductance (Novick et al., 2016), but only soil moisture should affect soil conductance (Lehmann et al., 2008; Merlin et al., 2016). In the m -order VPD model described above, the canopy conductance G_{veg} explicitly depends on VPD_l (Eq. (6)). We then sorted the G_s and GPP data into categories representing the 0–15th, 15–30th, 30–50th, 50–70th, 70–85th, and 85–100th percentiles of soil moisture, spanning a gradient of dry to wet condition at each site. The non-linear regression using ordinary least squares fit (OLS) was performed for Eq. (4) in each soil moisture category to find the fitted parameters (i.e. G_0 , G_1 and m) when there were more than 30 data points in any given category. Meanwhile, considering that there were errors in any of G_s , GPP and VPD, we also tested the regression results using total least squares fit (TLS) (Petras and Bednarova, 2010). G_{soil} and G_{veg} were then calculated in each soil moisture category, to evaluate their dependence on soil moisture. In each soil moisture category, we also applied a bootstrap approach to consider the uncertainties of the derived G_{soil} and G_{veg} . We randomly selected half of the total number of data points in each soil category and applied non-linear regression to derive G_{soil} . We performed 500 bootstrap simulations and thus obtained 500 occurrences of G_{soil} within each soil moisture category. G_{veg} not only varies with soil moisture but also varies with VPD_l and GPP. We thus took the mean value of G_{veg} for each bootstrap run. The residual analysis of the observed and estimated G_s was performed at each site to validate the non-linear regression model results.

We note that a simpler, binned VPD model, $G_s = G'_0 + G'_1 \cdot GPP$, which does not impose the exponential VPD dependence in the canopy conductance G_{veg} and does not lack VPD dependence on soil conductance, was also tested on the dataset. In this model, the data is categorized across all VPD_l and soil moisture conditions. A linear regression with GPP is performed in each VPD_l -soil moisture category. In other words, the functional form of the vegetation conductance on VPD_l is not assumed nor imposed. In this binned VPD model, in addition to soil moisture categories, we further sorted the data on the basis of VPD_l with a width of 0.2 kPa within each soil moisture category to reflect the conductance dependence on VPD_l . There were $j = 1, 2, \dots, N_i$ VPD_l

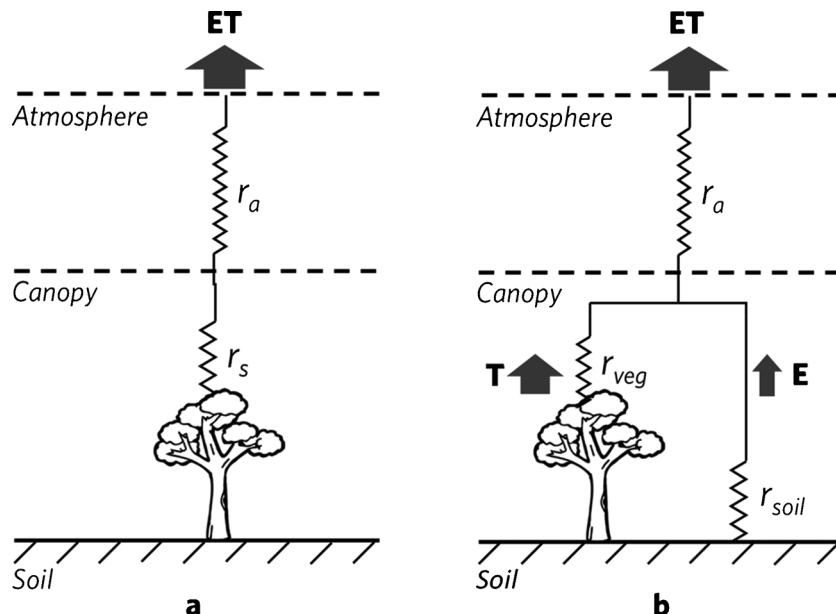


Fig. 1. The conceptual framework of different ET models. **a** Structure of the Penman-Monteith model, and **b** Shuttleworth-Wallace model. r_a is aerodynamic resistance, r_s is ecosystem surface resistance, r_{veg} is canopy surface resistance, and r_{soil} is soil surface resistance. All resistances are the inverse of conductances.

categories in each soil moisture category, where N_i varies with the maximum VPD_l observed at each site. The linear regression was performed in each category to find the best fitted parameters (i.e. intercept G_0' , and slope G_1'), which were then used to calculate G_{veg} and G_{soil} .

2.4. Evapotranspiration partitioning

Once we have separated soil and canopy conductances, we can use them to partition evaporation and transpiration as in dual-source ET models. Fig. 1a shows the structure of the PM model, which treats the surface with a single resistance (inverse of ecosystem conductance). Our partitioning method, based on soil and canopy conductance, is similar to resistance in parallel (Fig. 1b) (Shuttleworth and Wallace, 1985). We can then relate total ET to the partitioning using flux conservation:

$$ET \cdot r_s = E \cdot r_{soil} = T \cdot r_{veg} \quad (7)$$

Where r_s is ecosystem surface resistance = $1/G_s$, r_{veg} is canopy surface resistance = $1/G_{veg}$, and r_{soil} is soil surface resistance = $1/G_{soil}$.

So that we get the partitioning:

$$\frac{T}{ET} = \frac{r_s}{r_{veg}} = \frac{G_{veg}}{G_s} \quad (8)$$

$$\frac{E}{ET} = \frac{r_s}{r_{soil}} = \frac{G_{soil}}{G_s} \quad (9)$$

We note that $E/ET + T/ET$ always equals to 1 by definition.

2.5. Leaf area index (LAI) and Dryness Index (DI)

To analyze the effect of vegetation coverage on ET partitioning, LAI ($m^2 m^{-2}$) was estimated from PAR data, following (Xu et al., 2010):

$$LAI = -\frac{1}{k} \ln(1 - fPAR) \quad (10)$$

$$fPAR = 1 - \frac{PAR_{out}}{PAR_{in}} \quad (11)$$

Where k is taken as 0.5 here (Lin et al., 2018), fPAR is the fraction of absorbed photosynthetically active radiation, PAR_{out} and PAR_{in} are the outgoing and incoming photosynthetically active radiation ($W m^{-2}$), respectively.

Dryness index (DI) is calculated as the ratio of net radiation to the energy equivalent of precipitation (Kleidon et al., 2014).

3. Results

3.1. Ecosystem conductance variations

The impacts of soil moisture on G_{soil} and G_{veg} are shown in Fig. 2 at three sites, namely US-ARM (CRO), FR-LBr (ENF), DE-Gri (GRA). Boxplots in each soil moisture category display the uncertainties of the derived G_{soil} and G_{veg} using the bootstrap approach. As expected, lower data density was accompanied by higher uncertainty when using non-linear regression, emphasizing the importance of sufficient statistics. Nonetheless, the uncertainty in derived G_{soil} and G_{veg} was well-constrained in general. The residuals, $G_{residual}$, of the non-linear regression model in each soil moisture category all displayed a random pattern with zero mean, suggesting that the regression results are satisfactory. The higher residual observed in the lower data density category again emphasizes the importance of data quantity. The G_{soil} values, which should be strongly influenced by soil moisture, increased with soil moisture at 21 sites, and the trends were significant at 15 sites (p -value < 0.05) (Fig. 3b). Meanwhile, G_{soil} increased with soil moisture in various degrees across sites which may due to different soil types (Fig. 3a). We additionally showed that G_{soil} did not vary systematically with either radiation or VPD_l (Figure S1), this is consistent with our physical understanding for G_{soil} which should only depend on soil moisture but not on VPD (Or et al., 2013). 22 sites showed increasing trend in G_{veg} with soil moisture, 11 of which were significant (p -value < 0.05) (Fig. 3d). In fact, G_{veg} varies with both soil moisture and VPD_l , but soil moisture and VPD_l are negatively correlated at long time-scales (Novick et al., 2016). Canopy conductance decreased with lower soil moisture and higher VPD_l in order to reduce water loss. A clear pattern of G_{veg} variations among different PFTs was found, with

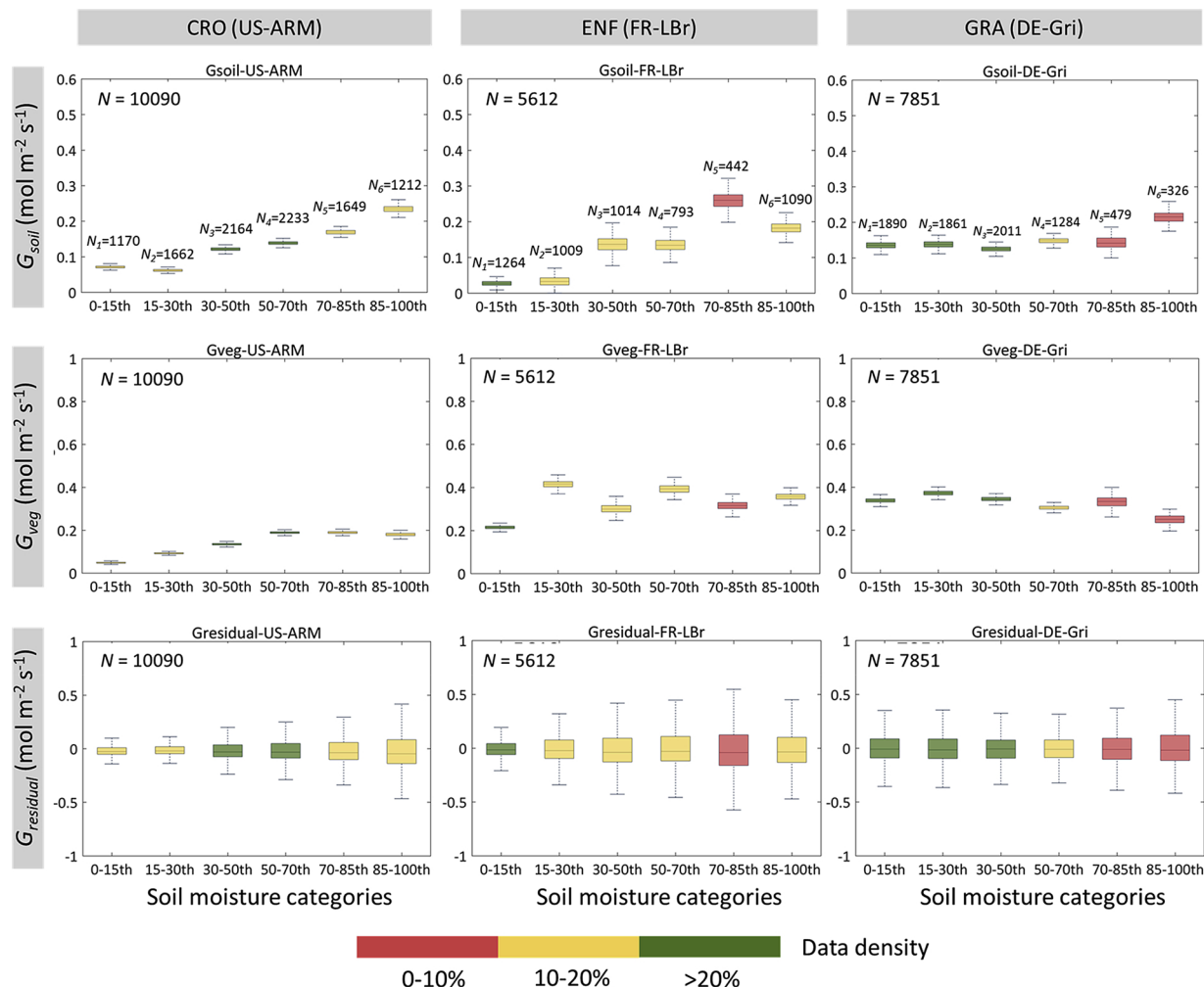


Fig. 2. Examples of variation in G_{soil} , G_{veg} , and $G_{residual}$ as a function of soil moisture at three sites. The number N in the upper left corner of each subplot indicates the total number of effective hourly data points used at each site after data screening. The number of effective data points within each soil moisture category (N_i) is labeled beneath the boxplots. Colors of the boxplots show the data density ($N_i/N*100\%$) for each soil moisture category at each site.

evergreen needleleaf forests having the largest G_{veg} , followed by deciduous broadleaf forests, croplands, grasslands and woody savannas (Fig. 3c).

3.2. Binned VPD model versus m -order VPD model

Hourly estimated G_s using the binned VPD model and m -order VPD model were compared to the G_s values inverted by PM equation at each site. For example, Fig. 4a and b depict the comparison of estimated G_{soil} and G_{veg} using the m -order VPD model and binned VPD model at all sites. The time series of G_s and G_{veg} at the DE-Gri site are further shown in Fig. 4c and d. Differences between the two models were minimal, indicating the validity of our exponent model assumption to separate soil and canopy conductances. The similarity of the models also confirms that G_{soil} is not dependent on VPD as the binned VPD model matches the m -order VPD method well, and the latter has no VPD dependence for G_{soil} .

In Figure S2 we compare results of G_{soil} , G_{veg} and $T:ET$ using either

the OLS or TLS methods. We did not observe much difference between these two methods across the 30 sites used in this study.

3.3. Estimation of ET partitioning

Next we investigate the $T:ET$ distribution for different PFTs (Fig. 5). We compared $T:ET$ for evergreen needleleaf forests, croplands and grasslands where sample sites are sufficient. The average $T:ET$ was higher for evergreen needleleaf forests than the other two PFTs, with a value of 0.75 ± 0.17 . Croplands exhibited a lower $T:ET$ from 0.36 to 0.84 with a mean of 0.62, followed by grasslands with $T:ET$ of 0.56 ± 0.15 . There were only two sample sites representing woody savannas and one sample site representing evergreen broadleaf forests, where the estimated $T:ET$ were 0.61 ± 0.09 and 0.54, respectively. The average $T:ET$ for deciduous broadleaf forests was 0.8 at three sites with a standard variation of 0.09.

Thereafter, seasonal and interannual variations in $T:ET$ were estimated at the daily scale. Time series of these values are shown in Fig. 6

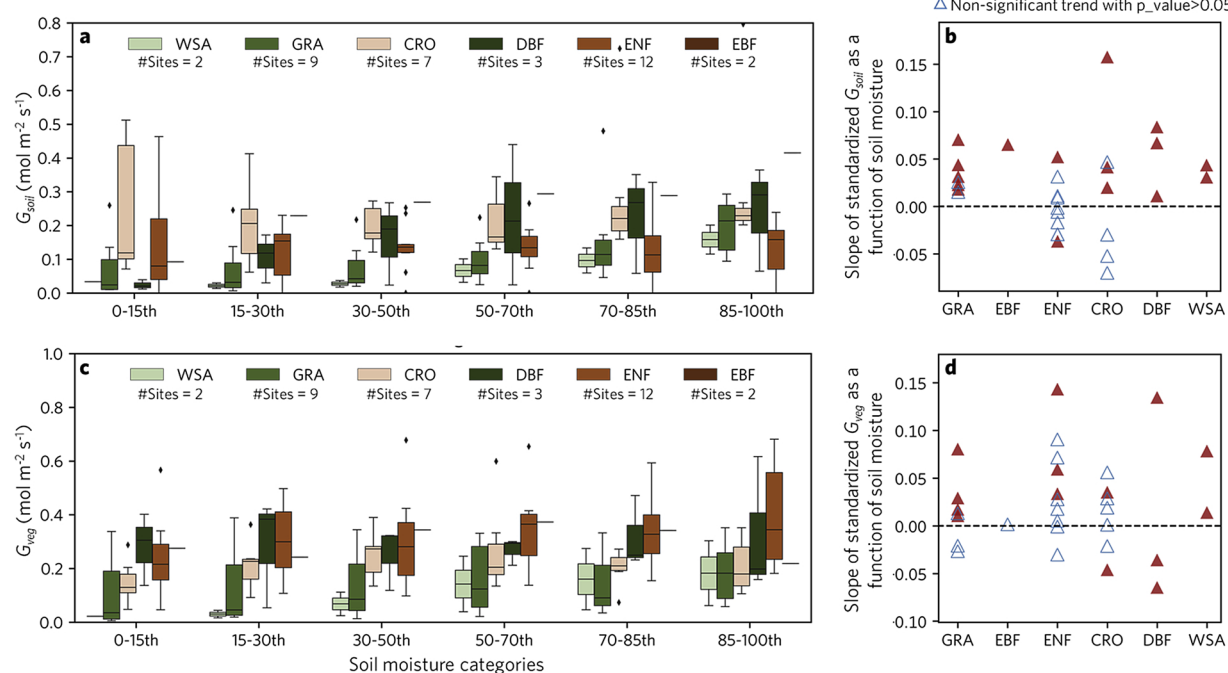


Fig. 3. Variations of G_{soil} and G_{veg} with soil moisture across PFTs at all 30 sites. a, c The G_{soil} and G_{veg} as a function of soil moisture. Boxplots show the distributions of G_{soil} and G_{veg} at different sites for the same PFT. #Sites indicate the number of sites for different PFTs. **b, d** The slope of standardized G_{soil} and G_{veg} as a function of soil moisture at all 30 sites. Variables were standardized by dividing maximum values. A positive slope indicates an increasing trend of variables as a function of soil moisture and vice versa.

for the US-NR1 (ENF), US-Ne1 (CRO), DE-Gri (GRA), and IT-Col (DBF) sites. The vegetation at the US-NR1 site is dominated by subalpine mixed evergreen coniferous forest. Daily variations of $T:ET$ at US-NR1 were about 0.05–0.2 in the pre-growing season, but showed larger day-to-day variations and reached to values of 0.54 ± 0.2 during the growing season. The vegetation cover changed slightly within a year at the evergreen site, so that the variability of $T:ET$ could be largely attributed to other biotic and abiotic factors, such as weather and soil moisture dynamics (Berkelhammer et al., 2016). The shape of $T:ET$ at US-Ne1 site shows that croplands grow faster compared to other natural plants and transpiration reach maximum rapidly. At DE-Gri, high $T:ET$ lasts for a longer period, suggesting a longer growing season for grasslands. $T:ET$ at the peak growing season is highest for deciduous broadleaf forests at IT-Col site with the values close to 1.

3.4. Energy balance effect

Table S3 shows the regression coefficients between ($LE + H$) and the available energy ($R_n - G$). Ideal energy closure is represented by an intercept of 0 and a slope of 1 (Wilson et al., 2002). We can see that the slope is close to 1 for all site-years, ranging from 0.82 to 1.06, with a mean of 0.99 ± 0.05 . The intercept ranged from -18.86 to 40.65 W m^{-2} , with a mean of $14.83 \pm 14.98 \text{ W m}^{-2}$. The results imply a generally good energy closure in the data used here. However, the effect of unclosed energy balance to the inverted G_s and the corresponding $T:ET$ is non-negligible. Fig. 7 shows the mean diurnal variation of G_s and corresponding $T:ET$ at the US-AR2 site which has a minimum slope of 0.82. The energy balance ratio (EBR), defined as $(LE + H) / (R_n - G)$ is less than 1 for most conditions and displays an

increasing trend from the morning to the evening with the energy balance being nearly closed in the late afternoon (Fig. 7a). By assigning the residual entirely to either H , LE or $(R_n - G)$, we can assess the maximum uncertainty in G_s arising from the non-closure of the surface energy balance. As shown in Fig. 7b, G_s estimates in all three cases are identical when EBR equals 1 and deviate when EBR is lower or higher than 1. When $EBR < 1$, assuming that all errors are in H , we obtain the lowest G_s values. In contrast, when assuming that all errors are in LE , the overestimated LE leads to the highest G_s estimates, which is up to about 200% higher than the reference case (in which all errors were assumed to be in H). The uncertainty in G_s propagates to the uncertainty in $T:ET$, yet to lesser extent. Similar to the behavior of G_s , errors in LE also have the largest impact on $T:ET$ estimation. However, the maximum uncertainty in $T:ET$ is much less than G_s . The lowest $T:ET$ when assuming that all errors are attributed to LE is only 14% less than $T:ET$ estimation in the reference case. This can be explained in part by modification of the canopy conductance G_{veg} as well and in part by the reduction of the response of $T:ET$ to the EBR in the regression. Although the magnitude of $T:ET$ is affected by the closure of the energy balance, the diurnal course of $T:ET$ shows similar behavior in all three cases. The same analysis was also applied to all sites and we find that the overall $T:ET$ among all sites is 0.60 ± 0.14 by assuming all errors are in LE , 9% lower than but close to the original $T:ET$ estimated by assuming all EBR errors originated from H (0.66 ± 0.15).

3.5. Effect of LAI on $T:ET$

The relationship between mean annual $T:ET$ and mean growing season LAI at different sites is shown in Fig. 8. The linear regression

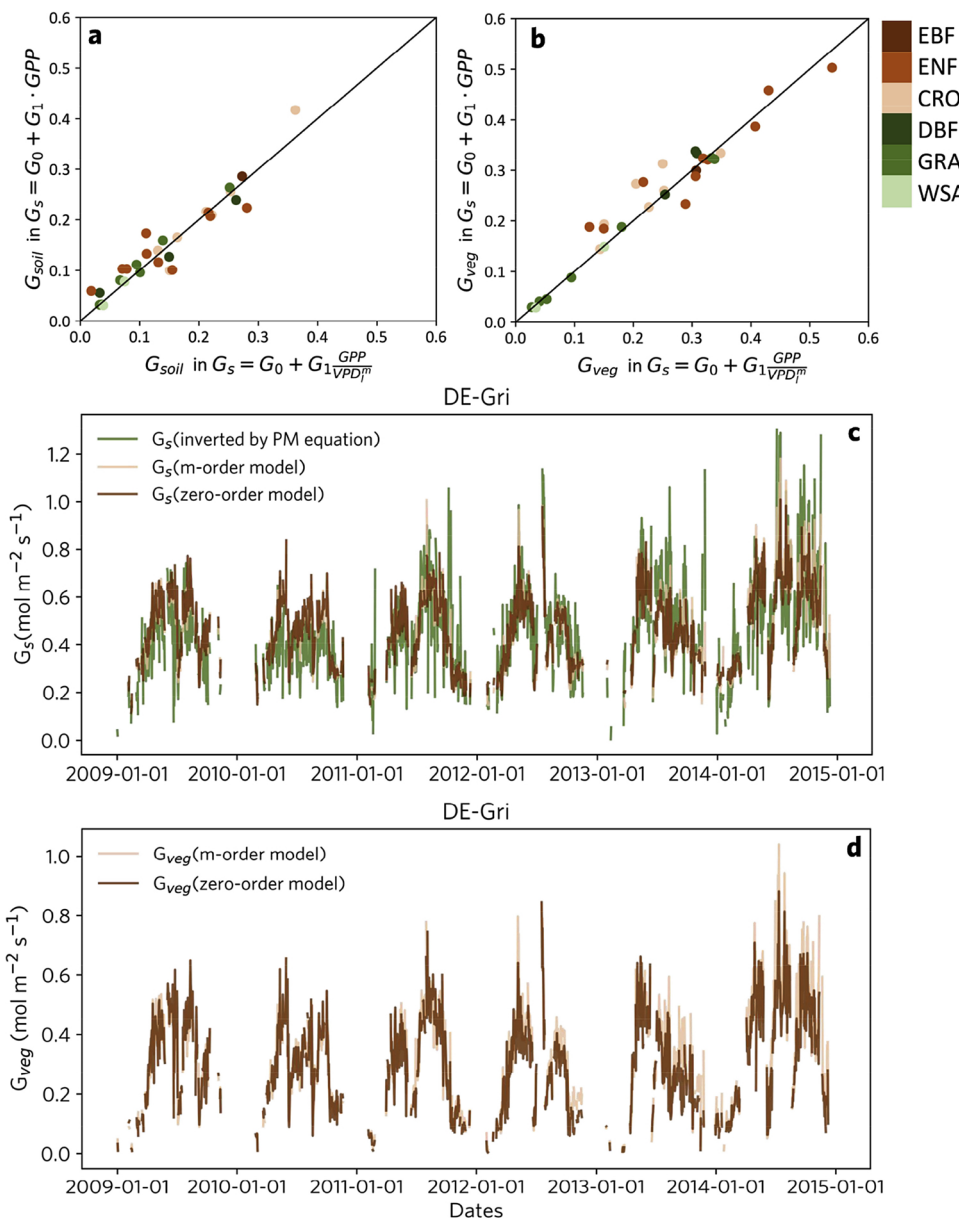


Fig. 4. The comparison between observed and estimated conductances using the *m*-order VPD model and binned VPD model. **a, b** Mean G_{soil} and G_{veg} comparison across all 30 sites. **c** Daily G_s comparison at DE-Gri site. **d** Daily G_{veg} comparison at DE-Gri site.

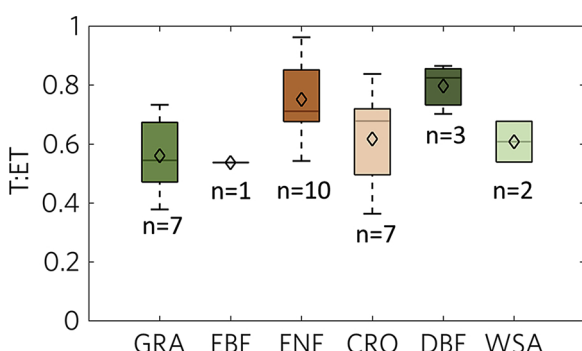


Fig. 5. Distributions of mean annual $T:ET$ for 30 sites across different PFTs. The diamond and solid line in the boxes refer to the average and median values, respectively. The n value below each boxplot indicates the number of sites for each PFT.

between $T:ET$ and estimated mean LAI shows a significant R^2 (p -value = 0.01), reflecting some regulation of vegetation coverage on $T:ET$ variability across biomes. More precisely, locations with less vegetated areas typically resulted in lower $T:ET$. However, the low R^2 of 0.2 suggested that mean LAI only has minimal explanatory power for $T:ET$ variability across biomes, and additional factors are at play.

Seasonal variation of $T:ET$ with LAI at individual sites was then examined. LAI values were categorized into bins with widths of 0.05. This width is arbitrary but reflects a trade-off between large enough bins for sufficient statistics in each category and small enough ones to capture a seasonal signal. Mean $T:ET$ in each LAI category was calculated and the relationship between $T:ET$ and LAI at four typical sites with different PFTs are shown in Fig. 9. Results at all 30 sites are shown in Figure S3. We note that the LAI deduced from the measured fPAR ranges between 2 and 8 m² m⁻² in the growing season, with an absence

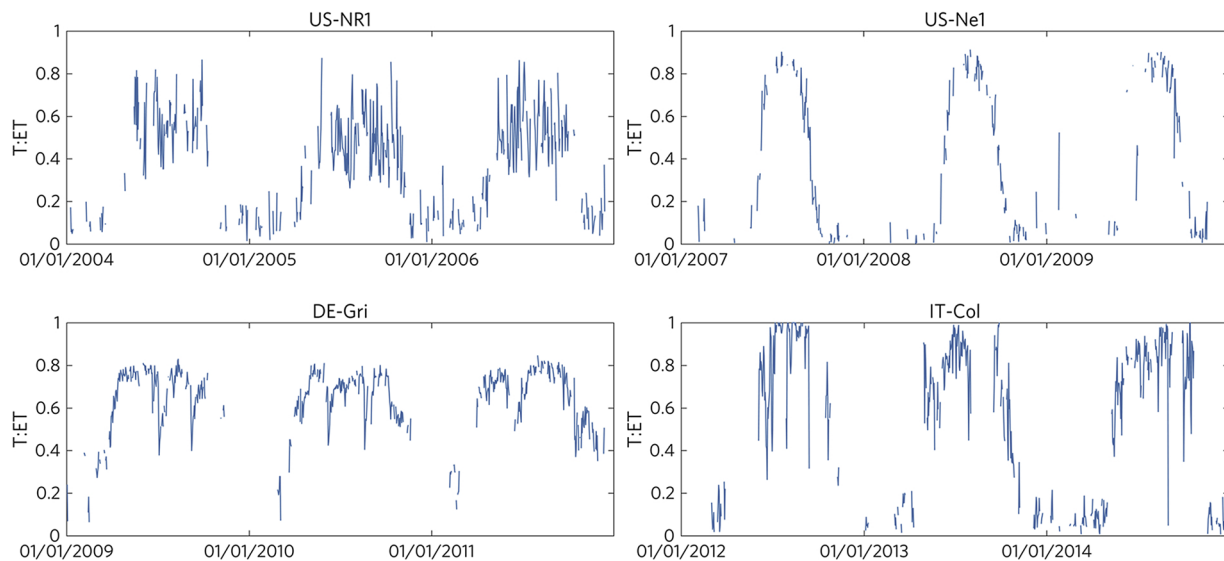


Fig. 6. Seasonal and interannual variation of T:ET at the daily scale for the US-NR1 (ENF), US-Ne1 (CRO), DE-Gri (GRA), IT-Col (DBF) sites.

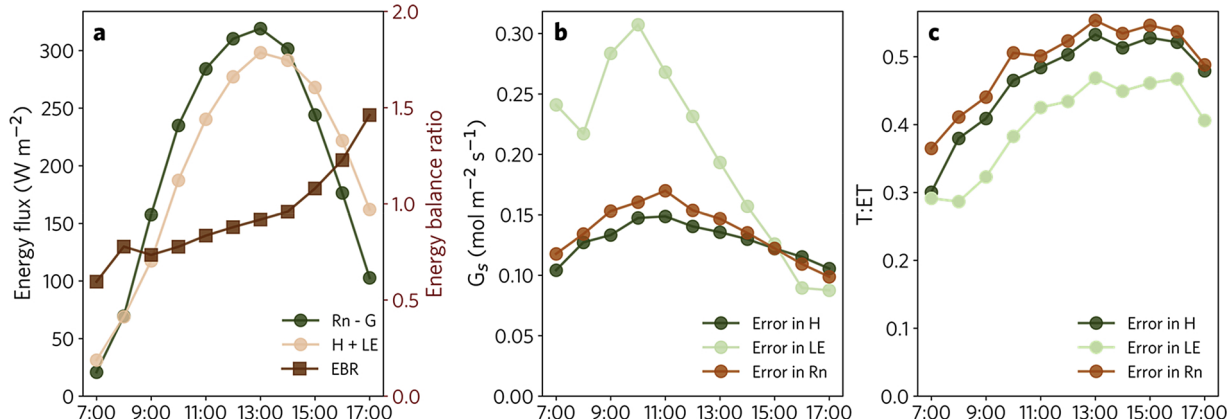


Fig. 7. Mean diurnal variation (over all available site years) of (a) energy fluxes and the energy balance ratio, (b) ecosystem surface conductance, and (c) the corresponding T:ET for the site US-AR2.

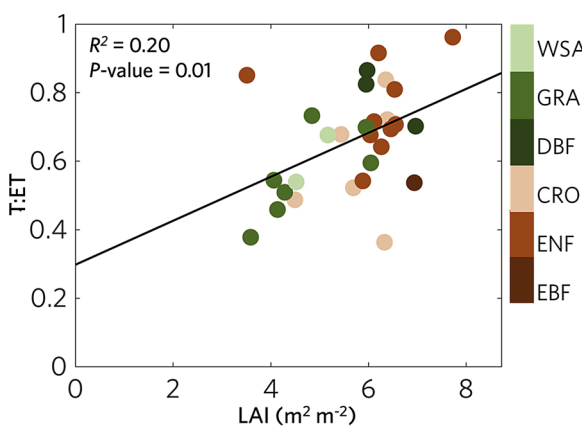


Fig. 8. Scatter plot between mean annual T:ET and mean growing season LAI per site. The black solid line shows the fitted linear regression ($R^2 = 0.20$, $p\text{-value} = 0.01$) for all sites between T:ET and LAI.

of very low values. The lack of low LAI values can be explained by the fact that the measured broadband fPAR rapidly saturates (Zhang et al., 2018), and thus has extremely high values and exhibits minimal variations throughout the year at many sites (Figure S4). Despite this, we found a nonlinear increase of T:ET with LAI. At low to medium LAI, as expected, T:ET values were relatively constant and evaporation was by far the main contributor to total ET. After that, T:ET increased sharply with LAI, suggesting that vegetation coverage controls T:ET at seasonal scales. It is noteworthy that T:ET did not reach 1 even at the highest LAI, emphasizing that evaporation within the eddy-covariance footprint could still be important even at very high vegetation coverages.

3.6. Effect of precipitation and dryness index on T:ET

The linear regression showed a low and non-significant R^2 ($p\text{-value} = 0.11$) between T:ET and mean annual precipitation with a value of about 0.09 (Fig. 10a), in agreement with both observational evidence (Schlesinger and Jasechko, 2014) and modeling result (Fatichi

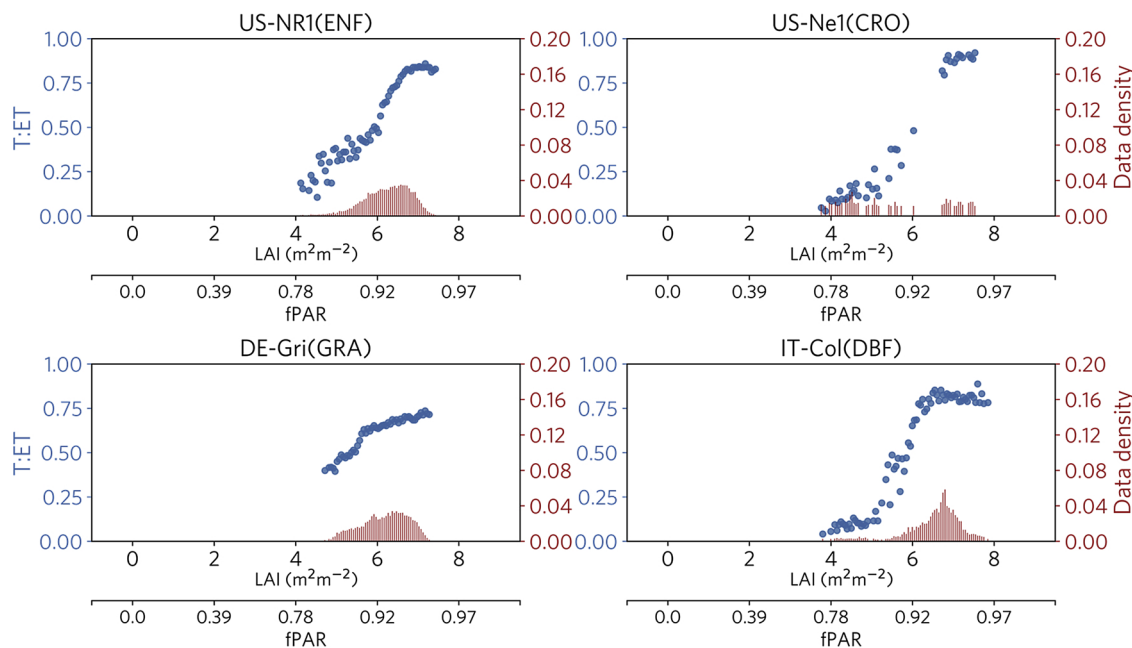


Fig. 9. The variation of $T:ET$ along with fPAR induced LAI at four sites. Dots in the figure are mean $T:ET$ at each LAI category with a width of 0.05. Bar plot shows the data density at each LAI category.

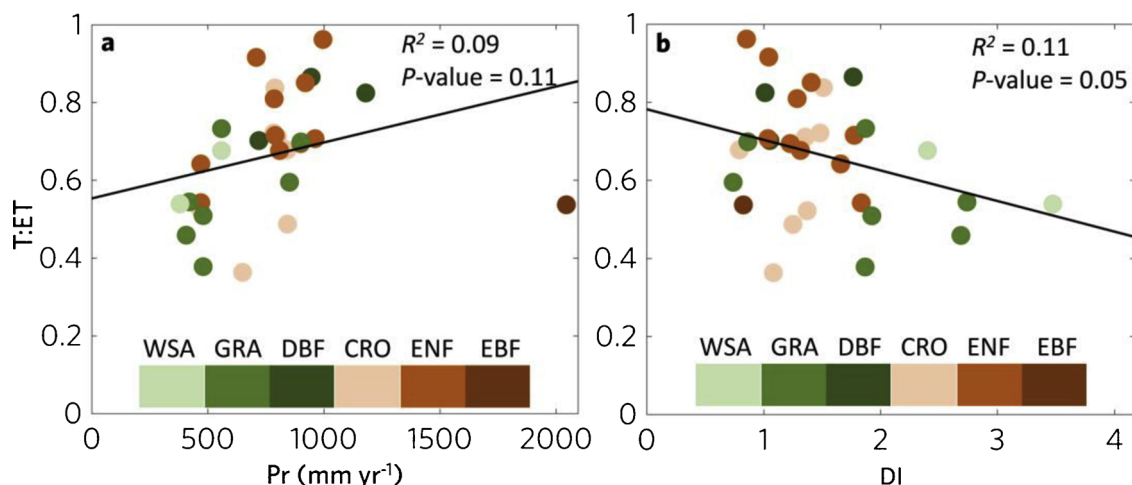


Fig. 10. Scatterplots between mean annual $T:ET$ and (a) the mean annual precipitation (Pr , mm yr^{-1}), (b) dryness index (DI) per sites. Annual fluxes averaged over the entire data period are presented. The black lines show the fitted linear regressions.

and Pappas, 2017). We performed a similar analysis for the DI. Fig. 10b shows that $T:ET$ was generally higher in wet climates than dry ones ($R^2 = 0.11$, p -value = 0.05).

While long-term precipitation impact may be small, we also consider the effect of rainfall pulses on the temporal variations of E . Sites having rain-free periods lasting at least 10 days were chosen. For example, Fig. 11 shows the estimated daily E with rainfall pulses at US-SRG and US-SRM sites. Soil E increased sharply right after each rainfall event, followed by slower, decaying trends. The evaporation rate is

approximately proportional to the square root of inverse time after a rainfall event. Low and relatively steady E was found during long periods without precipitation, reflecting the fact that evaporation from a relatively dry soil becomes very restricted. This phenomenon was only clearly observable at US-SRG and US-SRM sites, where the rainfall frequencies are low and have fewer disturbing effects on soil evaporation rates. In addition, the slope of decreasing evaporation rate after rainfall varied across sites, which likely reflects various soil pore properties (Brutsaert, 2014).

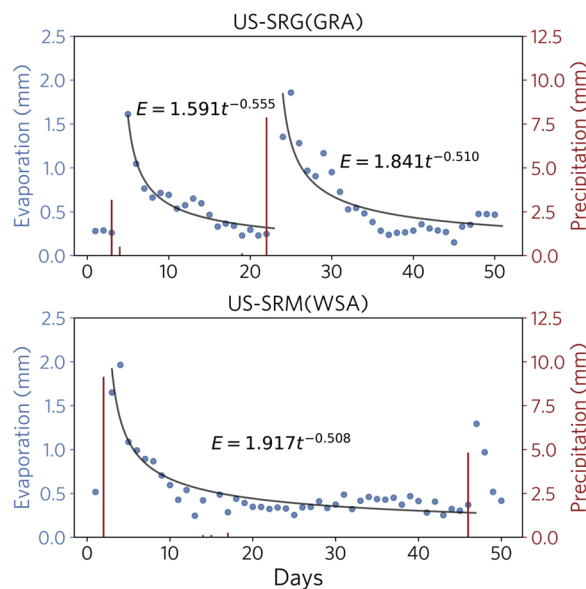


Fig. 11. Daily variation of evaporation at US-SRG and US-SRM sites. Bar plots show the rainfall pulses. The equations inserted in subplots show the evaporation rate with time t (in days) after a certain rainfall event.

4. Discussion

4.1. Response of ecosystem conductances to soil moisture

The observed increase of G_{soil} and G_{veg} with soil moisture and of the latter with decreasing VPD are consistent with physical understanding on soil conductance (Lehmann et al., 2008; Merlin et al., 2016) and canopy conductance (Novick et al., 2016). Canopy conductance responses to soil moisture are dependent on the hydraulic strategies of plants and are predicted to be tightly coupled to the xylem anatomy of a particular species and the vulnerability of that xylem to cavitation

(Huntingford et al., 2015; Anderegg et al., 2017). Declines in soil moisture lead to xylem embolism and subsequent loss of xylem hydraulic conductance (Prior and Eamus, 2000; Chen et al., 2008). These results of soil and canopy conductances were not imposed but arise naturally from the analysis, confirming the validity of our method to separate ET. Furthermore, comparison of estimated G_{veg} and G_{soil} between the m -order VPD model and the binned VPD model confirms the assumption in our method that G_{soil} is not VPD dependent. Both the m -order VPD model and binned VPD model can be used to separate conductances; however, there are tradeoffs between the two. First, the regression results are highly influenced by the number of data points. From this perspective, the m -order VPD model will be resilient to statistics as it requires values limited to a soil moisture bin rather values limited by both soil moisture and VPD binning. Second, the binned VPD model does not impose a non-linear VPD dependence in G_{veg} and thus could be more flexible to describe the relationship between G_{veg} and VPD since this relationship is not yet fully understood. The evaluation of the G_s regression results could be helpful in choosing between different models, yet overall at our sites we did not find difference between the two retrievals (Fig. 4).

4.2. Comparison with other independent ET partitioning methods

Mean annual $T:ET$ across all sites were compared with previous published estimates using several different methods (Fig. 12). The average $T:ET$ in this study ($66 \pm 15\%$) is very close to a recent model simulation (Fatichi & Pappas, 2017) and results using isotopic methods (Good et al., 2015), but a little higher than other published values based on eddy-covariance data estimates and meta-analysis. We further compared the estimated mean annual $T:ET$ with reported values for different PFTs (Fig. 5). The estimated $T:ET$ for evergreen needleleaf forests in this study (0.75 ± 0.17) is higher than that reported in Zhou et al. (2016) (0.59 ± 0.06) and Schlesinger and Jasechko (2014) (0.55 ± 0.15), but close to the simulation of Fatichi and Pappas (2017) at FLUXNET sites (0.71 ± 0.07). $T:ET$ for the same PFT is marginally affected by the total number of selected sites. Uncertain observations and large variability across sites can generate a large range of $T:ET$ as discussed in Wang et al. (2014) and may explain why the $T:ET$ estimates for the same PFT differ so much among different studies. The range of $T:ET$ for croplands (0.62 ± 0.16) is within the range for this vegetation type reported in Zhou et al. (2016) ($0.53 - 0.75$). The $T:ET$ in grasslands (0.56 ± 0.15) is also very similar to that reported in Zhou et al. (2016) (0.56 ± 0.05) and Schlesinger and Jasechko (2014) (0.57 ± 0.19). Thus, our estimated mean annual $T:ET$ is within the range of previous estimates for the three different vegetation types (ENF, CRO, and GRA). As for the remaining three vegetation types (EBF, DBF, and WSA), we unfortunately do not have enough sites to support comparisons.

For additional validation, we compared our estimates of mean annual $T:ET$ at seven single sites with values reported in Fatichi and Pappas (2017) and Scott and Biederman (2017). Table 1 shows that our estimated annual $T:ET$ is fairly similar to those reported in the literature. These broad comparisons give an idea of where our new method for ET partitioning falls among existing ones.

4.3. Controlling factors of ET partitioning

Apart from the uncertainties in flux measurements and in the non-

Fig. 12. $T:ET$ range in this study, as well as in previously published literature. Solid bold lines within colored bars highlight the mean estimate of $T:ET$ for each study, while boxes extend to plus-minus a standard deviation, or to the reported ranges in the published literature. The reported studies apply different methods for estimating $T:ET$: (i) Wang et al. (2014) and Schlesinger and Jasechko (2014) provided synthesis analyses of published studies; (ii) Zhou et al. (2016) used eddy-covariance data with correlations between carbon and water flux; (iii) Maxwell and Condon (2016) and Fatichi and Pappas (2017) were based on mechanistic ecohydrological models; and (iv) Good et al. (2015) was based on isotopic analysis.

Table 1
Comparison of mean annual $T:ET$ at seven different sites.

Source	DE-Hai	IT-Ren	IT-SRO	NL-Loo	US-SRG	US-SRM	US-Wkg
This study	0.70	0.68	0.81	0.79	0.55	0.54	0.46
Fatichi and Pappas (2017)	0.69	0.71	0.73	0.72	—	—	—
Scott and Biederman (2017)	—	—	—	—	0.55	0.62	0.46

linear regression method, other biotic and abiotic factors, such as vegetation cover, water, and energy availability, all contribute to the observed variations of $T:ET$ across sites. Our results show that LAI could explain 20% of the variation in $T:ET$ across sites. T is strongly affected by biological factors, such as vegetation coverage, while the remaining component ($ET - T$) is more influenced by abiotic processes which are composed of observational uncertainty, the ignored interception evaporation (Fatichi and Pappas, 2017; Wei et al., 2017), and climatic conditions such as precipitation and the aridity index (Zhu et al., 2015). However, temporal variations of $T:ET$ show strong dependence on LAI at each site. We noted that $T:ET$ does not tend to 1 at high vegetation coverage, which emphasizes the inaccuracy of assuming that T equals ET at very high LAI. It could also reflect the presence of open water bodies within the footprint of the flux measurement. In agreement with Schlesinger and Jasechko (2014) and Fatichi and Pappas (2017), the correlation between $T:ET$ and aridity index is weak and negative, while that between $T:ET$ and mean annual precipitation across sites was essentially zero. However, soil evaporation variations directly reflect precipitation pulses (Knauer et al., 2017). The evolution of soil evaporation rate can be divided into three distinct processes: an initially high and relatively constant rate that is supported by internal capillary flow, a slowing and decaying trend controlled by soil hydraulics, and finally a low and relatively steady value because of the diffusion-limited vapor transport (Mutziger et al., 2005; Or et al., 2013; Brutsaert, 2014). As described in Brutsaert (2014), evaporation rate after a precipitation event follows a $t^{-0.5}$ law, with t the time after rainfall. This soil evaporation theory is well reflected in our inversion at some sites, further confirming that our method correctly reproduces expected physical results.

4.4. Implications and limitations

Our study shows that the $T:ET$ ratio can be estimated at routine eddy-covariance towers, with a few simple assumptions, namely: (1) Ecosystem surface conductance is assumed to be the sum of soil and canopy conductance; (2) Transpiration through canopy conductance is related to photosynthesis; (3) Minimum canopy conductance due to cuticular and epidermal losses is negligible; and (4) Equation (7) is set up by assuming that surface temperatures for vegetation and soil are the same. Compared to other partitioning techniques using eddy-covariance measurements, our method has several advantages. Unlike the approach proposed by Scanlon and Kustas (2010), we do not require a priori knowledge of plant water use efficiency, a factor that is difficult to determine in practice and highly variable across environmental conditions species. Contrary to Zhou et al. (2016), we neither assume a given VPD dependence nor enforce that T would be equal to ET at points during the growing season, an assumption that may be violated in water-limited areas with sparse vegetation. Contrary to Scott and Biederman (2017), we do not need multiyear data and thus our method can be used anytime during the year. The novelty of the current work is to use an objective (either m -order VPD model or binned VPD model) and simple method for $T:ET$ partitioning, based on the fact that canopy conductance is directly proportional to GPP. It is a data-driven method that can be applied to routine eddy-covariance observations in all conditions, accounting for soil moisture and environmental variations.

However, there are still limitations in this study. First, when considering total ecosystem surface conductance as the sum of the soil and canopy conductance in the proposed method, we are implicitly assuming that surface temperature is the same for the entire canopy and soil. Although it is not a perfect approximation, it is not critical as the GPP used is the one at the ecosystem scale and thus incorporates the vertical profile of light and turbulence in the canopy, so that only the soil component remains. Second, rainfall interception evaporation was excluded, as the instability of flux data observations during those periods make it a difficult value to extract. Third, the uncertainty of eddy-covariance measurements, including closure issues and the corrected

GPP estimation based on net ecosystem exchange data generate uncertainties in the estimate. Finally, the parameters derived from non-linear regression are affected by the number of data points: sites with few data points would result in some uncertainties in the parameters and hence in the $T:ET$ estimates.

5. Conclusions

This study has used half-hourly meteorological and ecosystem flux data from 30 eddy-covariance sites to develop a simple new ET partitioning method based on a series of simple assumptions. We first separated the inverted ecosystem surface conductance into canopy and soil conductance using a regression method based on either an m -order VPD model or binned VPD model. The separated canopy and soil conductances were then used to calculate $T:ET$ using the concept of dual-source ET models.

The separated canopy and soil conductances deduced from the data in this study were both highly regulated by soil moisture, in agreement with our physical understanding and validating our assumptions in separating conductances. The mean annual $T:ET$ deduced from the separated conductances varied among different vegetation types, with the highest value for evergreen needleleaf forests (0.75 ± 0.17), followed by croplands (0.62 ± 0.16) and grasslands (0.56 ± 0.15). An un-closed energy balance, especially errors in LE, highly affects the inverted G_s and corresponding $T:ET$ results. In this study, the lack of energy balance closure issue caused about 9% uncertainties on the overall $T:ET$ among all sites. Mean growing season LAI displayed a relatively low explanatory power on spatial variations of $T:ET$. However, the correlation between LAI and $T:ET$ become evident at the seasonal scale within a given site, where $T:ET$ increased nonlinearly with LAI. Even at the highest LAI, $T:ET$ still did not extend all the way to 1, revealing that the evaporation is not negligible even at a high vegetation coverage. There was no significant relationship between $T:ET$ versus precipitation across sites; however, the estimated evaporation rate from this study correctly reflected the temporal variations of soil evaporation after precipitation pulses.

As this new ET partitioning method provides a simple and objective way to estimate $E:ET$ and $T:ET$, it could be readily applied to global flux tower networks for monitoring ecosystem dynamics and hydrological responses to environmental change. The derived $T:ET$ can also be further used to assess the water use efficiency for different ecosystems in the future.

Acknowledgments

The 2015 FLUXNET data was available online (<http://fluxnet.fluxdata.org/>). This work used eddy-covariance data acquired and shared by the FLUXNET community, including these networks: AmeriFlux, AfriFlux, CarboAfrica, CarboEuropeIP, CarboItaly, CarboMont, ChinaFlux, Fluxnet-Canada, GreenGrass, ICOS, KoFlux, LBA, NECC, OzFlux-TERN, TCOS-Siberia, and USCCC. This work was financially supported by the National Natural Science Foundation of China (Grant Nos. 91225301 and 91425303). Xi Li is grateful for China Scholarship Council for the financial support of a twelve-months study at Columbia University. Pierre Gentile acknowledges funding from NASA17-THP17-0036 “Remote sensing estimate of evapotranspiration partitioning to transpiration”, as well as funding from DOE Early Career grant.

Appendix A. Supplementary data

Supplementary material related to this article can be found, in the online version, at doi:<https://doi.org/10.1016/j.agrformet.2018.11.017>.

References

- Anderegg, W.R.L., Wolf, A., Arango-Velez, A., et al., 2017. Plant water potential improves prediction of empirical stomatal models. *PLoS One* 12, 1–17.
- Baldocchi, D.D., Ryu, Y., 2011. A synthesis of forest evaporation fluxes—from days to years—as measured with eddy covariance. *Forest Hydrology and Biogeochemistry*. Springer, pp. 101–116.
- Ball, J.T., Woodrow, I.E., Berry, J.A., 1987. A model predicting stomatal conductance and its contribution to the control of photosynthesis under different environmental conditions. *Progress Photosynthesis Res.* 221–224.
- Berkelhammer, M., Noone, D.C., Wong, T.E., et al., 2016. Convergent approaches to determine an ecosystem's transpiration fraction. *Glob. Biogeochem. Cycles* 30, 933–951.
- Brutsaert, W., 2014. The daily mean zero-flux plane during soil-controlled evaporation: a Green's function approach. *Water Resour. Res.* 50, 9405–9413.
- Cammalleri, C., Rallo, G., Agnese, C., Ciraolo, G., Minacapilli, M., Provenzano, G., 2013. Combined use of eddy covariance and sap flow techniques for partition of ET fluxes and water stress assessment in an irrigated olive orchard. *Agric. Water Manag.* 120, 89–97.
- Chen, X., Rubin, Y., Ma, S., Baldocchi, D., 2008. Observations and stochastic modeling of soil moisture control on evapotranspiration in a Californian oak savanna. *Water Resour. Res.* 44, 1–13.
- Diarra, A., Jarlan, L., Er-Raki, S., et al., 2017. Performance of the two-source energy budget (TSEB) model for the monitoring of evapotranspiration over irrigated annual crops in North Africa. *Agric. Water Manag.* 193, 71–88.
- Farley, K.A., Jobbágy, E.G., Jackson, R.B., 2005. Effects of afforestation on water yield: a global synthesis with implications for policy. *Glob. Chang. Biol.* 11, 1565–1576.
- Fatichi, S., Pappas, C., 2017. Constrained variability of modeled $T : ET$ ratio across biomes. *Geophys. Res. Lett.* 44, 6795–6803.
- Foken, T., 2008. The energy balance closure problem: an overview. *Ecol. Appl.* 18, 1351–1367.
- Good, S.P., Soderberg, K., Guan, K., King, E.G., Scanlon, T.M., Taylor, K.K., 2014. 82H isotopic flux partitioning of evapotranspiration over a grass field following a water pulse and subsequent dry down. *Water Resour. Res.* 50, 1410–1432.
- Good, S.P., Noone, D., Bowen, G., 2015. Hydrologic connectivity constrains partitioning of global terrestrial water fluxes. *Science* 349, 175–177.
- Green, J.K., Konings, A.G., Alemanhammad, S.H., et al., 2017. Regionally strong feedbacks between the atmosphere and terrestrial biosphere. *Nat. Geosci.* 10, 410–414.
- Griffis, T.J., 2013. Tracing the flow of carbon dioxide and water vapor between the biosphere and atmosphere: a review of optical isotope techniques and their application. *Agric. For. Meteorol.* 174–175, 85–109.
- Huntingford, C., Smith, D.M., Davies, W.J., Falk, R., Sitch, S., Mercado, L.M., 2015. Combining the [ABA] and net photosynthesis-based model equations of stomatal conductance. *Ecol. Modell.* 300, 81–88.
- Jasechko, S., Sharp, Z.D., Gibson, J.J., Birks, S.J., Yi, Y., Fawcett, P.J., 2013. Terrestrial water fluxes dominated by transpiration. *Nature* 496, 347–350.
- Katul, G.G., Oren, R., Manzoni, S., Higgins, C., Parlange, M.B., 2012. Evapotranspiration: a process driving mass transport and energy exchange in the soil-plant-atmosphere-climate system. *Rev. Geophys.* 50.
- Kleidon, A., Renner, M., Porada, P., 2014. Estimates of the climatological land surface energy and water balance derived from maximum convective power. *Hydrol. Earth Syst. Sci.* 18, 2201–2218.
- Knauer, J., Zaelke, S., Medlyn, B.E., et al., 2017. Towards physiologically meaningful water-use efficiency estimates from eddy covariance data. *Glob. Chang. Biol.*
- Konings, A.G., Williams, A.P., Gentile, P., 2017. Sensitivity of grassland productivity to aridity controlled by stomatal and xylem regulation. *Nat. Geosci.* 10, 284–288.
- Kool, D., Agam, N., Lazarovitch, N., Heitman, J.L., Sauer, T.J., Ben-Gal, A., 2014. A review of approaches for evapotranspiration partitioning. *Agric. For. Meteorol.* 184, 56–70.
- Lee, D., Kim, J., Lee, K.S., Kim, S., 2010. Partitioning of catchment water budget and its implications for ecosystem carbon exchange. *Biogeosciences* 7, 1903–1914.
- Lehmann, P., Assouline, S., Or, D., 2008. Characteristic lengths affecting evaporative drying of porous media. *Phys. Rev. E – Stat. Nonlinear Soft Matter Phys.* 77.
- Lemordant, L., Gentile, P., Swann, A.S., Cook, B.I., Scheff, J., 2018. Critical impact of vegetation physiology on the continental hydrologic cycle in response to increasing CO_2 . *Proc. Natl. Acad. Sci.* 201720712.
- Leuning, R., 1995. A critical appraisal of a combined stomatal - photosynthesis model for C3 plants. *Plant Cell Environ.* 18, 339–355.
- Leys, C., Ley, C., Klein, O., Bernard, P., Licata, L., 2013. Detecting outliers: do not use standard deviation around the mean, use absolute deviation around the median. *J. Exp. Soc. Psychol.* 49, 764–766.
- Lhomme, J., Chehbouni, A., 1999. Comments on dual-source vegetation \pm atmosphere transfer models. *Agric. For. Meteorol.* 94, 269–273.
- Li, X., Zheng, Y., Sun, Z., et al., 2017. An integrated ecohydrological modeling approach to exploring the dynamic interaction between groundwater and phreatophytes. *Ecol. Model.* 356, 127–140.
- Lin, Y.S., Medlyn, B.E., Duursma, R.A., et al., 2015. Optimal stomatal behaviour around the world. *Nat. Clim. Chang.* 5, 459–464.
- Lin, C., Gentile, P., Huang, Y., Guan, K., Kim, H., Zhou, S., 2018. Diel ecosystem conductance response to vapor pressure deficit is suboptimal and independent of soil moisture. *Agric. For. Meteorol.* 250–251, 24–34.
- Lu, X., Liang, L.L., Wang, L., Jenerette, G.D., McCabe, M.F., Grantz, D.A., 2017. Partitioning of evapotranspiration using a stable isotope technique in an arid and high temperature agricultural production system. *Agric. Water Manag.* 179, 103–109.
- Mastrotheodoros, T., Pappas, C., Molnar, P., et al., 2017. Linking plant functional trait plasticity and the large increase in forest water use efficiency. *J. Geophys. Res. Biogeosci.* 122, 2393–2408.
- Maxwell, R.M., Condon, L.E., 2016. Connections between groundwater flow and transpiration partitioning. *Science* 353, 377–380.
- Medlyn, B.E., Duursma, R.A., Eamus, D., et al., 2011. Reconciling the optimal and empirical approaches to modelling stomatal conductance. *Glob. Chang. Biol.* 17, 2134–2144.
- Medlyn, B.E., De Kauwe, M.G., Lin, Y.S., et al., 2017. How do leaf and ecosystem measures of water-use efficiency compare? *New Phytol.*
- Merlin, O., Stefan, V.G., Amazirh, A., et al., 2016. Modeling soil evaporation efficiency in a range of soil and atmospheric conditions using a meta-analysis approach. *Water Resour. Res.* 52, 3663–3684.
- Monteith, J.L., 1965. Evaporation and environment. *Symp. Soc. Exp. Biol.* 19, 205–234.
- Mutziger, A.J., Burt, C.M., Howes, D.J., Allen, R.G., 2005. Comparison of measured and FAO-56 modeled evaporation from bare soil. *J. Irrig. Drain. Eng.-Asce* 131, 59–72.
- Novick, K.A., Ficklin, D.L., Stoy, P.C., et al., 2016. The increasing importance of atmospheric demand for ecosystem water and carbon fluxes. *Nat. Clim. Chang.* 6, 1023–1027.
- Or, D., Lehmann, P., Shahraeeni, E., Shokri, N., 2013. Advances in soil evaporation physics—a review. *Vadose Zone J.* 12, 0.
- Papale, D., Reichstein, M., Aubinet, M., et al., 2006. Towards a standardized processing of Net Ecosystem Exchange measured with eddy covariance technique: algorithms and uncertainty estimation. *Biogeosciences* 3, 571–583.
- Pastorello, G., Agarwal, D., Papale, D., et al., 2014. Observational data patterns for time series data quality assessment. *Proceedings - 2014 IEEE 10th International Conference on eScience, eScience 2014* 1, 271–278.
- Penman, H.L., 1948. Evaporation from open water, bare soils and grass. *Proc. R. Soc. Lond. Ser. A Math. Phys.* 193, 120–145.
- Petras, I., Bednarova, D., 2010. Total least squares approach to modeling: a Matlab toolbox. *Acta Montanistica Slovaca* 15, 158–170.
- Prior, L.D., Eamus, D., 2000. Seasonal changes in hydraulic conductance, xylem embolism and leaf area in *Eucalyptus tetrodonta* and *Eucalyptus miniatia* saplings in a north Australian savanna. *Plant Cell Environ.* 23, 955–965.
- Risi, C., Noone, D., Frankenberger, C., Worden, J., 2013. Role of continental recycling in intraseasonal variations of continental moisture as deduced from model simulations and water vapor isotopic measurements. *Water Resour. Res.* 49, 4136–4156.
- Scanlon, T.M., Kustas, W.P., 2010. Partitioning carbon dioxide and water vapor fluxes using correlation analysis. *Agric. For. Meteorol.* 150, 89–99.
- Scanlon, T.M., Sahu, P., 2008. On the correlation structure of water vapor and carbon dioxide in the atmospheric surface layer: a basis for flux partitioning. *Water Resour. Res.* 44, 1–15.
- Schlesinger, W.H., Jasechko, S., 2014. Transpiration in the global water cycle. *Agric. For. Meteorol.* 189–190, 115–117.
- Scott, R.L., Biederman, J.A., 2017. Partitioning evapotranspiration using long-term carbon dioxide and water vapor fluxes. *Geophys. Res. Lett.* 44, 6833–6840.
- Shuttleworth, W.J., Wallace, J.S., 1985. Evaporation from sparse crops—an energy combination theory. *Q. J. R. Meteorol. Soc.* 111, 839–855.
- Sun, Z., Zheng, Y., Li, X., et al., 2018. The Nexus of water, ecosystems, and agriculture in Endorheic River Basins: a system analysis based on integrated ecohydrological modeling. *Water Resour. Res.* 54.
- Tian, F., Qiu, G.Y., Yang, Y.H., Lü, Y.H., Xiong, Y., 2013. Estimation of evapotranspiration and its partition based on an extended three-temperature model and MODIS products. *J. Hydrol.* 498, 210–220.
- Wang, L., Good, S.P., Taylor, K.K., Cernusak, L.A., 2012. Direct quantification of leaf transpiration isotopic composition. *Agric. For. Meteorol.* 154–155.
- Wang, L., Good, S.P., Taylor, K.K., 2014. Global synthesis of vegetation control on evapotranspiration partitioning. *Geophys. Res. Lett.* 41, 6753–6757.
- Wei, Z., Yoshimura, K., Wang, L., Miralles, D.G., Jasechko, S., Lee, X., 2017. Revisiting the contribution of transpiration to global terrestrial evapotranspiration. *Geophys. Res. Lett.* 44, 2792–2801.
- Wen, X., Yang, B., Sun, X., Lee, X., 2016. Evapotranspiration partitioning through in-situ oxygen isotope measurements in an oasis cropland. *Agric. For. Meteorol.* 230–231, 89–96.
- Weng, E., Luo, Y., 2008. Soil hydrological properties regulate grassland ecosystem responses to multifactor global change: a modeling analysis. *J. Geophys. Res. Biogeosci.* 113.
- Williams, I.N., Lu, Y., Kueppers, L.M., Riley, W.J., Biraud, S.C., Bagley, J.E., Torn, M.S., 2016. Land-atmosphere coupling and climate prediction over the U.S. Southern great plains. *J. Geophys. Res.* 121 (12), 145 125–12.
- Wilson, K., Goldstein, A., Falge, E., et al., 2002. Energy balance closure at FLUXNET sites. *Agric. For. Meteorol.* 113, 223–243.
- Xu, D.Y., Kang, X.W., Zhuang, D.F., Pan, J.J., 2010. Multi-scale quantitative assessment of the relative roles of climate change and human activities in desertification – a case study of the Ordos Plateau, China. *J. Arid Environ.* 74, 498–507.
- Zhang, Y., Shen, Y., Sun, H., Gates, J.B., 2011. Evapotranspiration and its partitioning in an irrigated winter wheat field: a combined isotopic and micrometeorologic approach. *J. Hydrol.* 408, 203–211.
- Zhang, Y., Xiao, X., Wolf, S., et al., 2018. Spatio-temporal convergence of maximum daily light-use efficiency based on radiation absorption by canopy chlorophyll. *Geophys. Res. Lett.* 3508–3519.
- Zhou, S., Yu, B., Zhang, Y., Huang, Y., Wang, G., 2016. Partitioning evapotranspiration based on the concept of underlying water use efficiency. *Water Resour. Res.* 52, 1160–1175.
- Zhu, X.J., Yu, G.R., Hu, Z.M., et al., 2015. Spatiotemporal variations of T/ET (the ratio of transpiration to evapotranspiration) in three forests of Eastern China. *Ecol. Indic.* 52, 411–421.